IIETA International Information and Engineering Technology Association
Advancing the World of Information and Engineering

Mathematical Modelling of Engineering Problems
Vol. 10, No. 5, October, 2023, pp. 1706-1716
Journal homepage: http://iieta.org/journals/mmep

Hybrid Algorithm of Backpropagation and Relevance Vector Machine with Radial Basis Function Kernel for Hydro-Climatological Data Prediction

Syaharuddin[1,2], Fatmawati[1*], Herry Suprajitno[1], Ibrahim[3]

[1] Department of Mathematics, Faculty of Science and Technology, Universitas Airlangga, Surabaya 60115, Indonesia
[2] Department of Mathematics Education, Faculty of Teacher Training and Education, Universitas Muhammadiyah Mataram, Mataram 83127, Indonesia
[3] Department of Geography Education, Faculty of Teacher Training and Education, Universitas Muhammadiyah Mataram, Mataram 83127, Indonesia

Corresponding Author Email: fatmawati@fst.unair.ac.id

https://doi.org/10.18280/mmep.100521

Received: 13 April 2023
Revised: 8 July 2023
Accepted: 10 September 2023
Available online: 27 October 2023

Keywords:
backpropagation, relevance vector machine, radial basis function, hydro-climatological data, climate changes

ABSTRACT

Hydro-climatological data serves a pivotal role in monitoring climatic alterations and facilitating agricultural planning, inclusive of evapotranspiration estimation, water management, and crop pattern design. The necessity to accurately and expeditiously model and forecast this data underscores the need for effective methodologies. This paper introduces a hybrid algorithm, integrating backpropagation and relevance vector machine (BP-RVM) with a radial basis function (RBF) kernel. A comparative analysis was conducted between RBF and Logsig activation functions in conjunction with resilient backpropagation (trainrp) and Levenberg-Marquardt backpropagation (trainlm). The algorithm was employed to predict and categorize rainfall, temperature, wind speed, humidity, and sunshine duration data. Through extensive trials, the architecture parameters in the training-testing process of the BP-RVM algorithm were meticulously determined. Mean squared error (MSE) and mean absolute percentage error (MAPE) values were classified as indicating high forecast accuracy (<10%). Despite the RBF-trainlm kernel function combination exhibiting a faster epoch completion rate, the BP-RVM algorithm with the RBF-trainrp kernel function combination is recommended for future data prediction stages due to its lower error generation. The BP-RVM-RBF-trainrp algorithm outperformed BP-RVM-RBF-trainlm, with an average error difference of 1.39% in the training process and 2.28% in the testing process. The identified algorithms and architectures present potential for future applications in evapotranspiration calculation and crop pattern planning based on hydro-climatological data.

1. INTRODUCTION

Prediction methodologies are crucial in systematically estimating future occurrences based on historical and current data, thereby minimizing errors, or deviations between actual events and predicted outcomes [1]. Optimal prediction doesn't necessitate pinpointing the precise future event, but rather, it aims to provide the closest possible approximation [1]. As such, the selection of optimal modeling and computational methods is integral for creating a mathematical model capable of accurately studying and approximating true data [2].

Hydroclimatological data, encompassing rainfall, humidity, temperature, wind speed, and sunshine duration, serve as critical parameters in weather change monitoring and climate classification [3]. These data are particularly pertinent in agricultural planning, affecting cropping patterns [4-7]. Accurate prediction of these data necessitates the use of suitable methods, such as artificial neural networks (ANN), which are capable of processing multiple data inputs [8].

Among the various types of ANN, including perceptron and multilayer perceptron (MLP), backpropagation ANN possesses a more comprehensive architecture with the inclusion of more than one hidden layer [9]. This type allows for the processing of more data with an m×n matrix size and employs accuracy parameters like learning rate and momentum to expedite data training and testing [10]. ANNs have been extensively utilized in the prediction of time-series data [11, 12].

Irawan et al. [13] developed a computing system based on MATLAB GUI for predicting hydroclimatological data using backpropagation. This system was designed to determine irrigation water requirements and optimize profit in crop rotation planning in Lombok, Indonesia. However, the system's prediction and optimization methods were separate, limiting its ability to perform calculations swiftly and accurately.

Sachindra et al. [14] conducted a comparative study of climate change prediction and analysis through 48 observation stations in Australia using genetic programming (GP), ANN, support vector machine (SVM), and relevance vector machine (RVM) methodologies. The results favored RVM with a Polynomial kernel, attributable to its probabilistic prediction process that enhances classification accuracy [15]. RVM can generate models with structures and parameterizations that align with the data's informational content [16] and can make predictions utilizing varied kernel functions, such as radial

basis functions [17].

Furthermore, radial basis networks might necessitate more neurons than standard feedforward backpropagation networks but can often be designed in a fraction of the time [18]. This finding aligns with the research of Song et al. [19], which demonstrated that radial basis function neural networks (RBFNN) can outperform algorithms such as adaptive backpropagation (ABP), Levenberg-Marquardt (LM), and Quasi-Newton (QN), achieving a Kappa coefficient value of 0.943. Nitze et al. [20] also showed that SVM with a radial basis function kernel outperformed ANN and random forest (RF) algorithms in plant species classification, achieving an accuracy rate of 95%. Lastly, Ghorbani et al. [21] reported RBFNN superiority over SVM for river flow prediction.

Despite the significant strides made in climate prediction, pattern recognition, and classification, the combination of the backpropagation (BP) algorithm and relevance vector machine (RVM) to enhance computational systems has yet to be thoroughly explored. BP has been implemented in time series forecasting using existing training and activation functions with two hidden layers. Conversely, the RVM algorithm, trained solely with the radial basis function (RBF) kernel, lacks any hidden layers. As such, the amalgamation of these two algorithms could have noteworthy implications for architectural construction, introducing an array of training functions.

The use of the RBF as the kernel function in RVM also warrants exploration as an activation function in the backpropagation network. This research aims to assess the utility of the RBF function as an activation function in comparison to the commonly used logsig function in BP. To this end, the authors have integrated the backpropagation and relevance vector machine (BP-RVM) algorithm, juxtaposing two activation functions—RBF and logsig. Additionally, the resilient backpropagation (trainrp) and Levenberg-Marquardt backpropagation (trainlm) training functions were also simulated to discern the most effective architecture during the data training-testing process.

The evaluation of architectural accuracy will hinge on the number of epochs or iterations, as well as the Mean Squared Error (MSE), and Mean Absolute Percentage Error (MAPE) values generated during the training and testing process. This accuracy indicator is crucial in selecting the superior architecture. The proposed algorithm combination was designed with a five-layered network architecture, comprising an input layer, three hidden layers, and an output layer, to ascertain the efficacy of multiple layers during the data training and testing process.

Subsequently, the BP-RVM algorithm with the optimal combination of training function and activation function will be employed to forecast rainfall, temperature, humidity, wind speed, and sunshine duration data. The forecast results of each data set will be analyzed to discern patterns and classifications, offering insights into ongoing climate change. This research is poised to introduce a novel concept in the prediction and classification of hydroclimatological data, providing an initial foundation for planning future cropping patterns.

2. THEORETICAL BACKGROUND

2.1 Neural network backpropagation

Machine learning is an application of artificial intelligence (AI) or artificial neural network (ANN) disciplines that use statistical techniques to generate a mathematical model from a set of data through a structured computing system to learn to recognize data patterns [22]. One of the machine learning algorithms is backpropagation (BP) neural network. Backpropagation is a supervised learning algorithm and is usually used by perceptrons with many layers to change the weights connected to the neurons in the hidden layer [23]. Therefore, data prediction y_k can be determined by formula:

$$y(x) = f\left(w_{0k} + \sum_{j=1}^{p} w_{jk} \cdot f\left(v_{0j} + \sum_{i=1}^{n} v_{ij} \cdot x_i \right) \right) \quad (1)$$

where, x_1, x_2, ..., x_i, ..., x_n are an input layer determined by the amount of input data, y_1, y_2,..., y_k, ..., y_m are an output layer, z_1, z_2, ..., z_j, ..., z_p are hidden layers of multi-layer nature, v_{oj} is the initial weight matrix on the hidden layer that initializes randomly between 0 and 1, w_{0k} is the initial weight matrix on the output layer, while $f(.)$ is an activation function that converts input data into external data between layers in intervals of -1 and 1, depending on the activation function given at each layer [24].

Backpropagation architecture uses activation functions and training functions to improve the performance of the constructed network. Logsig sigmoid activation functions perform better than tansig and purelin [25]. These results were obtained when performing 27 combinations of logsig, tansig, and purelin functions with two hidden layers. Based on the results of the training data, it was found that using the logsig function in each hidden layer gave the highest performance compared to random combinations. Meanwhile, the commonly used training functions with good accuracy are resilient backpropagation [26], and Levenberg-Marquardt backpropagation [27-32]. The results of these studies concluded that the trainlm function was able to generate fewer epochs than the trainrp function, but had a negative impact on the network error value during the data training process. In accordance with these theories and research results, we utilized a backpropagation architecture with three hidden layers and a logsig activation function. Furthermore, this function was combined with the training functions trainrp and trainlm to determine the accuracy of each function. We did not train the data using other combinations of functions that exist in the theory of the backpropagation algorithm.

2.2 Relevance vector machine

Michael E. Tipping was the first person to introduce Relevance Vector Machine (RVM) [33]. RVM is a machine learning method adapted from the Bayesian Framework. In addition, RVM has similarities with Support Vector Machine (SVM) in terms of function model. Like SVM, RVM was developed for binary analysis [15]. Another opinion stated that RVM is a probabilistic non-linear model with a prior distribution of weights that maintains sparsity [34]. On regression problems, RVM makes predictions based on functions [35]. RVM has been widely used in the field of prediction and classification [16, 36-43]. The RVM formula to determine prediction results is shown by Eq. (2) as follows:

$$y(x) = \sum_{i=1}^{n} v_i f(x_i) + v_0 \quad (2)$$

with x_i as input data, v_0 as bias matrix, v_i as weight matrix, $f(.)$ as kernel function, and n as amount of data [44]. There are three Kernel functions used in the simulation of RVM method, namely polynomial function, binary sigmoid function (logsig), and radial basis function (RBF) [45, 46]. However, the most commonly used functions are logsig as shown by Eq. (3) and RBF as shown by Eq. (4):

$$y(x) = \frac{1}{1+e^{-x}} \tag{3}$$

$$y(x) = \exp\left(-\frac{\|x-c\|^2}{2\cdot\sigma^2}\right) \tag{4}$$

Radial basis function (RBF) has been widely used as a kernel function. Swati et al. [47] utilized RBF on extreme learning machine (ELM) algorithm for classification of microarray data with 82.47% accuracy. Liu et al. [38] while conducting their research obtained a root mean square (RMS) value of 0.1025 with a running time of 1.435 seconds. This result is supported by Yu et al. [48], which showed that the determination coefficient of the RBF kernel was 0.924 (92.4%) in the data training process, whereas that of the Polynomial kernel was 0.411 (41.1%). Meanwhile, in the testing process, the determination coefficient of the RBF kernel reached 0.918 and that of the Polynomial kernel was 0.516. Lastly, Chen et al. [35] applied RBF for probabilistic prediction of concrete dam displacement and obtained an accuracy of 99.86%. Kara et al. [49] conducted experiments by comparing kernel polynomial and RBF by simplifying $(1/2 \cdot \sigma^2)=\gamma$ in Eq. (4) with any parameter, namely γ={0,0.1,0.2,0.3,0.4,...,5.0}. Furthermore, Nitze et al. [20] also experimented with the value of γ value of 0.01, whereas Wei et al. [50] used a γ value of 0.05. For that reason, we used the smallest γ value of 0.01 for each training and testing data. This simplification process was also conducted by Song et al. [19] when comparing ANN and SVM for land cover classification. Therefore, substituting the RBF formula into the RVM prediction function will result in the following Eq. (5):

$$y(x) = \sum_{i=1}^{n} v_i \cdot \exp\left(-\gamma\|x_i - c_i\|^2\right) + v_0 \tag{5}$$

with v_i as a weight matrix called the relevance vector, x_i as input data, γ as a free parameter for the kernel function [38, 51], c_i as the center of RBF. Razaque et al. [52] defines c_i value as the mean of the input data x_i. In addition, Razaque et al. [52] also formulated the Euclidean distance between each class and input matrix computationally according to Eq. (6):

$$D = \|x_i - c_i\|^2 = x_i^T c_i - \frac{1}{2} c_i^T c_i \tag{6}$$

Thus, the RVM formula with RBF kernel function for data prediction was obtained as shown by Eq. (7).

$$y(x) = \sum_{i=1}^{n} v_i \cdot \exp\left(-\gamma \cdot D\right) + v_0 \tag{7}$$

3. RESEARCH METHOD

3.1 Dataset

The authors utilized secondary data in the case study sourced from the Kediri station of West Lombok district, Indonesia at a latitude of 08˚-38'-11.0" S and a longitude of 116˚-10'-13.8" E. The data has been obtained and validated by a team of analysts from the West Lombok Meteorology, Geophysics and Climatology Agency. The data was obtained from field observation data through hydro-climatological data recording tools. Data is tabulated by year and month. The data were collected every 10 days, so there were 36 inputs in a year. The data were divided into 80% for data training and 20% for data testing, so the training data were taken from 2012 to 2019, while the testing data were collected from 2020 to 2021. The training and testing prediction input matrices are as follows.

$$\underbrace{\begin{bmatrix} x_1 & x_2 & x_3 & x_4 & x_5 & x_6 & x_7 & x_8 & x_9 & x_{10} & x_{11} & x_{12} & \cdots & x_{36} \\ x_2 & x_3 & x_4 & x_5 & x_6 & x_7 & x_8 & x_9 & x_{10} & x_{11} & x_{12} & x_{13} & \cdots & x_{37} \\ x_3 & x_4 & x_5 & x_6 & x_7 & x_8 & x_9 & x_{10} & x_{11} & x_{12} & x_{13} & x_{14} & \cdots & x_{38} \\ \vdots & \vdots & \vdots & \vdots & \vdots & \vdots & \vdots & \vdots & \vdots & \vdots & \vdots & \vdots & \cdots & \vdots \\ x_{252} & x_{253} & x_{254} & x_{255} & x_{256} & x_{257} & x_{258} & x_{259} & x_{260} & x_{261} & x_{262} & x_{263} & \cdots & x_{287} \end{bmatrix}}_{Input} \underbrace{\begin{bmatrix} x_{37} \\ x_{38} \\ x_{39} \\ \vdots \\ x_{288} \end{bmatrix}}_{T}$$

From the training data matrix arrangement, it is known that the input data are x_1, x_2, x_3, x_4, x_5, x_6, x_7..., x_{286}, x_{287}, while the target data (T) are x_{37}, x_{38}, x_{39}, x_{40}, x_{41}, ..., x_{288}, with data x_1, x_2, x_3, ..., x_{288} being actual data from 2012 to 2019. Furthermore, the testing data matrix arrangement is as follows.

$$\underbrace{\begin{bmatrix} x_{289} & x_{290} & x_{291} & x_{292} & x_{293} & x_{294} & x_{295} & x_{296} & x_{297} & x_{298} & x_{299} & x_{300} & \cdots & x_{324} \\ x_{290} & x_{291} & x_{292} & x_{293} & x_{294} & x_{295} & x_{296} & x_{297} & x_{298} & x_{299} & x_{300} & x_{301} & \cdots & x_{325} \\ x_{291} & x_{292} & x_{293} & x_{294} & x_{295} & x_{296} & x_{297} & x_{298} & x_{299} & x_{300} & x_{301} & x_{302} & \cdots & x_{326} \\ \vdots & \vdots & \vdots & \vdots & \vdots & \vdots & \vdots & \vdots & \vdots & \vdots & \vdots & \vdots & & \\ x_{324} & x_{325} & x_{326} & x_{327} & x_{328} & x_{329} & x_{330} & x_{331} & x_{332} & x_{333} & x_{334} & x_{335} & \cdots & x_{359} \end{bmatrix}}_{Input} \underbrace{\begin{bmatrix} x_{325} \\ x_{326} \\ x_{327} \\ \vdots \\ x_{360} \end{bmatrix}}_{T}$$

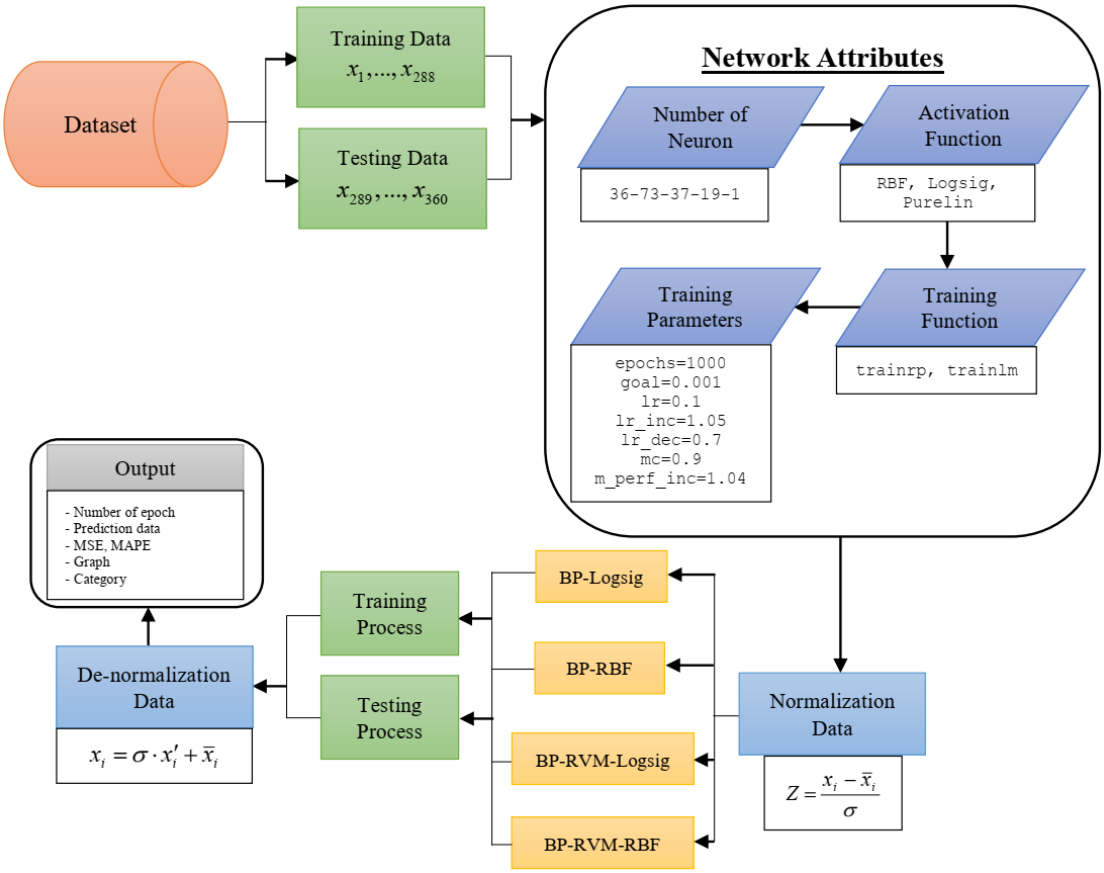

Figure 1. Research flowchart

From the testing data matrix arrangement, it is known that the input data are x_{289}, x_{290}, x_{291}, ..., x_{359}, while the target data (T) are x_{325}, x_{326}, x_{327}..., x_{360}, with data x_{289}, x_{290}, x_{291}, ..., x_{360} being actual data from 2020 to 2021. The training and testing process was used to find the best architecture with the combination of learning rate, momentum, activation function, and the appropriate training function that has the highest accuracy. Furthermore, this architecture was used for 2022 data prediction in the data prediction stage that utilized data collected for 10 years from 2012 to 2021.

3.2 Research procedure

Generally, the authors tried to combine BP and RVM algorithms with trainrp, trainlm, and RBF kernel functions. However, during the training and testing process, simulations were also carried out using the logsig training function and trainrp activation function to compare the accuracy of the constructed architecture. The training, testing, and prediction process used the Matlab graphical user interface (GUI). The diagram of the data training and testing process is shown in Figure 1.

Figure 1 compares that the experiments in this research are divided into three algorithm combinations including BP, BP-RVM, and BP-RVM-RBF. In the initial stage, we divided the data into two parts, namely training data (80%) and testing data (20%). Furthermore, the architecture used is three hidden layers with a formation of 36-73-37-19-1. This architecture is based on the results of research Syaharuddin et al. [53] when comparing seven formulas recommended by other researchers. The training and testing data used showed the results that in determining the number of neurons on the hidden-1 layer, it was more appropriate to use the Hecht-Nelson formula.

In the initial stage, we divided the data into two parts, namely training data (80%) and testing data (20%). Furthermore, the architecture used three hidden layers with 36-73-37-19-1 formation. This architecture was based on the results of the research conducted by Syaharuddin et al. [53] that compared seven formulas recommended by other researchers. The training and testing results showed that in determining the number of neurons on the first hidden layer, it was more appropriate to use the Hecht-Nelson formula (N_y=2 · N_x+1) whereas the Lawrence & Fredricson formula (N_y=0.5 · (N_{z1}+N_y)) was more suitable to be used on the second and third hidden layer. Thus, Syaharuddin et al. [24] recommended the following formula for the three hidden layers:

$$y(x) = f_O\left(wb_{0k} + \sum_{r=1}^{t} wb_{rk} \cdot f_{H3}\left(wa_{0r} + \sum_{q=1}^{s} wa_{qr} \cdot f_{H2}\left(w_{0q} + \sum_{j=1}^{p} w_{jq} \cdot f_{H1}\left(v_{0j} + \sum_{i=1}^{n} v_{ij} \cdot x_i\right)\right)\right)\right) \quad (8)$$

with v_{ij} as the weight on the first hidden layer, w_{jq} as the weight on the second hidden layer, wa_{qr} as the weight on the third hidden layer, wb_{rk} as the weight on the output layer, $f_O(.)$ as the activation function and purelin function on the output layer, $f_{H1}(.)$ as the logsig function on the first hidden layer, $f_{H2}(.)$ as the logsig function on the second hidden layer, and $f_{H3}(.)$ as the logsig function on the third hidden layer. In this study, the radial basis function was tested as the activation function, so it

would be compared with logsig, while the training function used trainrp and trainlm. The architecture training parameters included a goal of 0.001, a learning rate of 0.1, a momentum of 0.9, and other parameters in default position [54]. Finally, data normalization and de-normalization techniques utilized the Z-score formula according to Eq. (9):

$$Z = \frac{x_i - \bar{x}_i}{\sigma} \tag{9}$$

with x_i representing input data, $\bar{x}_i$ representing the mean of data, and σ representing the standard deviation of data. Furthermore, the formula for de-normalization is $x_i = \sigma \cdot x_i^{'} + \bar{x}_i$, with $x_i^{'} = Z$. This normalization technique is also supported by the research results of Abhishek et al. [55] on rainfall data prediction and Ogasawara et al. [56] on an experiment with non-stationary time series data approaches. The research results of Khond [57] and Nayak et al. [58] also proved that the Z-score normalization technique is better than min-max, decimal scaling, median, median-MAD, sigmoid, and tanh estimators. Finally, the output of the training process included prediction data, accuracy parameters (MSE & MAPE), graphical approximation of actual data and prediction data, and classification data according to predetermined conditions.

3.3 Classification of hydro-climatological data

The data used in this study were hydro-climatological data, including rainfall (mm), temperature (℃), wind speed (knots), humidity (%), and sunshine duration (%). The provisions for the classification of hydro-climatological data used the following theories:

a. Rainfall intensity characterizes climate change in an area. According to Wijaya et al. [59], if the method of Oldeman and Suardi [60] is utilized, climate can be classified by the intensity of rain or the nature of rain, namely wet months (WM) if the rainfall is >200 mm, humid months (HM) if rainfall is 100-200 mm, and dry months (DM) if the rainfall is <100 mm. Climate types can be seen by comparing the total number of DM and WM including. There are five types, namely A (10-12 WM), B (7-9 WM), C (5-6 WM), D (3-4 WM), and E (0-2 WM) [61].
b. Temperature classification based on the theory of Junghuhn [62] consists of cold regions (<11.1℃), cool regions (11.1℃-17.1℃), temperate regions (17.1℃-22℃), tropical regions (22℃-26.3℃), and hot regions (>26.3℃) [63, 64].
c. The classification of wind speed according to the Beaufort scale (1805) is divided into 8 types. However, taking into account the development of wind speed in the territory of Indonesia, the most common wind speed in the region is on the fourth scale, which is around 7 knots or 3.3-5.4 m/s (gentle breeze), characterized by the condition of leaves and twigs rippling [65]. Other classifications are calm (<1.5 m/s), light breeze (1.5-3.3 m/s), moderate breeze (5.4-10.7 m/s), strong breeze (10.7-13.8 m/s), near gale (13.8-17.1), strong gale (17.1-24.4), and hurricane (>24.4) [66, 67].
d. Humidity (%) is divided into three classifications, namely dry (<45%), ideal (45%-65%), and humid (>65%) [68, 69].
e. The classification of sunshine duration (%) was based on observations of four seasons, namely DJF (December, January, February), MAM (March, April, May), JJA (June, July, August), and SON (September, October, November). Observations were made in these months based on the length of sunshine for 12 hours [70, 71].

3.4 Architectural accuracy test

The number of epochs generated, Mean Square Error (MSE) and Mean Absolute Percentage Error (MAPE) were used in testing the accuracy of the developed network architecture. The MAPE category used the scale developed by [72]. A MAPE value of <10% indicates high accurate forecasting, 10% ≤ MAPE <20% indicates good forecasting, 20% ≤ MAPE <50% indicates reasonable forecasting, and 50% ≥ MAPE indicates inaccurate forecasting [73, 74]. The MSE and MAPE formulas are shown by Eq. (10) and Eq. (11):

$$MSE = \frac{1}{n}\sum_{i=1}^{n}\left(A_i - F_i\right)^2 \tag{10}$$

$$MAPE = \frac{1}{n}\sum_{i=1}^{n}\left|\frac{A_i - F_i}{A_i}\right| \times 100\% \tag{11}$$

with A_i representing the actual data, F_i representing the forecast data, and n representing the amount of data. In the data training and testing stages, the number of epochs, MSE and MAPE generated in each simulation were tabulated to facilitate the interpretation process. These parameters were used to find the best architecture for the prediction stage. The number of epochs was used to measure the duration of the training process by the architecture, the MSE value was utilized to check the average error of the architecture in recognizing actual data, while MAPE was used to classify whether the forecasting output was acceptable or rejected.

4. RESULT AND DISCUSSION

4.1 Formula of backpropagation-relevance vector machine

The difference between backpropagation and relevance vector machine is that the data process is operated by an activation function or kernel function. The kernel function used in this research was radial basis function. In backpropagation, each data x_i had to be multiplied by the v_i weight before being operated by the activation function (kernel). Meanwhile, in RVM, the x_i data was substituted into the kernel function before being multiplied by the v_i weight. Thus, if we refer to Eq. (8), the obtained BP-RVM formula for data prediction is as shown by Eq. (12).

$$y(x) = f_O\left(wb_{0k} + \sum_{r=1}^{t} wb_{rk} \cdot f_{H3}\left(wa_{0r} + \sum_{q=1}^{s} wa_{qr} \cdot f_{H2}\left(w_{0q} + \sum_{j=1}^{p} w_{jq} \cdot f_{H1}\left(v_{0j} + \sum_{i=1}^{n} v_{ij} \cdot f_I\left(x_i\right)\right)\right)\right)\right) \tag{12}$$

Eq. (12) shows that the x_i data before being input to the network must be substituted into Eq. (4), namely the RBF kernel function, so the data in the input layer is $f(x_i)$. In this study, a combination of RBF and logsig activation functions was utilized. The first hidden layer used RBF, while the second and third hidden layers used the logsig function. In addition, three sets of experiments were conducted: backpropagation with logsig activation function (BP), backpropagation with radial basis function (BP-RBF), and hybrid backpropagation-relevance vector machine with kernel radian basis function (BP-RVM-RBF). This experiment was constructed to see the reliability of each experiment based on the number of epochs it generates, the MSE value, and the MAPE value.

Table 1. Results of data training (80%) with BP and BP-RVM architecture

Algorithm	Function Activation	Function Training	Validation	Rainfall	Temperature	Air Humidity	Wind Speed	Sunshine
BP	Logsig	Trainrp	Epochs	50	75	63	73	77
			MSE	3,760.14	**0.2041**	12.039	1.63479	107.665
			MAPE (%)	-	**1.3317**	3.4053	22.3341	12.1253
		Trainlm	Epochs	7	**5**	7	6	5
			MSE	4,725.32	0.3070	22.519	3.11505	**84.1871**
			MAPE (%)	-	1.6055	5.0694	29.2333	**10.0764**
	RBF	Trainrp	Epochs	32	33	43	48	28
			MSE	**3,281.03**	0.3355	**8.2997**	**1.21556**	128.527
			MAPE (%)	-	1.8353	**2.9004**	**21.1533**	12.8816
		Trainlm	Epochs	5	6	7	6	5
			MSE	4,055.43	0.3073	19.456	3.35542	115.061
			MAPE (%)	-	1.6590	4.1715	32.0341	11.8795
BP-RVM	Logsig	Trainrp	Epochs	51	78	73	64	69
			MSE	3,288.56	0.2776	**8.7463**	3.11526	**50.8311**
			MAPE (%)	-	1.5457	**2.8498**	33.7935	**7.73501**
		Trainlm	Epochs	7	7	6	6	6
			MSE	5,010.87	0.2407	16.619	4.21556	89.6777
			MAPE (%)	-	1.5812	3.9722	41.3754	10.2614
	RBF	Trainrp	Epochs	34	34	29	39	27
			MSE	**1,899.38**	**0.1723**	11.914	**1.45861**	113.617
			MAPE (%)	-	**1.2278**	3.4890	**21.8947**	11.9119
		Trainlm	Epochs	4	5	6	6	4
			MSE	3,275.28	0.2100	10.840	3.05294	101.603
			MAPE (%)	-	1.3365	3.2103	27.5078	12.0518

Table 2. Results of data testing (20%) with BP and BP-RVM architecture

Algorithm	Function Activation	Function Training	Validation	Rainfall	Temperature	Air Humidity	Wind Speed	Sunshine
BP	Logsig	Trainrp	Epochs	20	18	17	17	20
			MSE	3,392.04	0.5158	6.9761	0.7830	236.02
			MAPE (%)	-	2.2349	2.5004	24.199	20.597
		Trainlm	Epochs	5	3	3	3	4
			MSE	**1,728.98**	0.4005	8.7887	1.2064	**182.24**
			MAPE (%)	-	1.9929	2.8904	28.434	**16.710**
	RBF	Trainrp	Epochs	14	13	14	14	14
			MSE	3,100.04	**0.2862**	**6.7194**	**0.3662**	244.02
			MAPE (%)	-	**1.5475**	**2.3186**	**15.639**	20.623
		Trainlm	Epochs	4	3	4	3	3
			MSE	4,361.39	0.3373	8.4527	1.0100	265.68
			MAPE (%)	-	1.8043	2.8381	28.730	22.564
BP-RVM	Logsig	Trainrp	Epochs	15	20	27	16	20
			MSE	**1,926.38**	0.3794	5.5811	**0.3165**	217.00
			MAPE (%)	-	1.9684	2.2245	**15.772**	19.656
		Trainlm	Epochs	5	4	4	3	3
			MSE	3,614.37	0.4206	10.455	0.8251	256.71
			MAPE (%)	-	1.9942	3.3266	23.084	21.257
	RBF	Trainrp	Epochs	15	13	13	16	15
			MSE	2,160.82	**0.3740**	4.9643	0.6858	**200.96**
			MAPE (%)	-	**1.7648**	2.0439	22.105	**18.065**
		Trainlm	Epochs	5	3	3	3	3
			MSE	3,891.34	0.4061	**4.6831**	1.1764	271.74
			MAPE (%)	-	1.9543	**1.9792**	28.575	20.618

4.2 Results of data training and testing

Training, testing, and data prediction processes were simulated using a Lenovo Intel(R) Core(TM) i5 CPU, M520, 2.40GHz, 8GB RAM. In the first step, training and testing data were divided with 80% of the actual data used for the training process and 20% for the testing process. The next step was making predictions using the best architecture. The dataset consisted of rainfall, temperature, wind speed, humidity, and sunshine duration. Hence, 20 experiments were carried out in each of the training and testing stages. Each training and testing output was tabulated as shown in Table 1.

Table 1 shows that the output of the backpropagation (BP) architecture with a combination of RBF activation functions had faster performance than the logsig function with relatively small MSE and MAPE values. The RBF-trainrp combination was able to speed up the training process almost twice as fast as the logsig-trainrp function. Meanwhile, the trainlm training function made the training process six times faster. However, the RBF-trainlm combination resulted in higher MSE and MAPE values than the RBF-trainrp function combination. This result was found in the rainfall, humidity, and wind speed data training process, each of which had the smallest MSE and MAPE values. Furthermore, the backpropagtion-relevance vector machine (BP-RVM) experiment with the RBF-trainrp function combination also showed better data training results than other function combinations. This combination obtained MSE value of 1,899.38 from rainfall data, MSE value of 0.1723 from temperature data, and MSE value of 1.459 from wind speed data. Meanwhile, the combination of logsig-trainrp functions for humidity and sunshine duration data training resulted in the smallest MSE and MAPE values. In general, the MAPE value of each data training result is still classified as indicating highly accurate forecasting. The results of data testing can be seen in Table 2.

Table 2 shows that the BP-RVM algorithm with the RBF-trainrp function combination had good performance. In the rainfall data testing stage, the MSE value was 2,160.82. This value is 10.85% greater than the MSE value obtained from the logsig-trainrp function. The smallest MSE and MAPE values of temperature and sunshine data were obtained from the RBF-trainrp function. Moreover, the smallest MSE value of air humidity data was obtained from the RBF-trainlm function, differed by 0.28 from the MSE value obtained from the RBF-trainrp function. Finally, the smallest MSE value of wind speed data was obtained from the logsig-trainrp function with a difference of 0.37 from the MSE from the RBF-trainrp function. The results of this analysis demonstrated that the BP-RVM algorithm with the RBF-trainrp function had better performance than other function combinations.

Another finding showed that the BP-RVM algorithm with RBF kernel function is better than the logsig function. This can be seen from the number of epochs generated in each experiment. The RBF-trainrp function obtained 13-16 epochs, while the logsig-trainrp function obtained 15-27 epochs. Another result demonstrated that the trainlm function can reduce the number of epochs to a maximum of 5 epochs. The small number of epochs generated from the trainlm function impacted the error values (MSE and MAPE) produced both during data training and testing. This result is in accordance with the findings of Kannaiyan et al. [29] when comparing response surface methodology (RSM) and artificial neural network (ANN) with trainlm function, namely RSM and ANN models are constructed from the experimental data and they are correlated reasonably well while having an R 2 value of 0.8468 and 0.9999 respectively. Furthermore, Ahmad et al. [30] also produced an accuracy for the levernberg marquardt training algorithm reaching 77.7%. this result is higher than gradient descent with momentum at 76.7% and resilient backpropagation at 73.3%. However, the error value generated by the trainlm function is greater than the trainrp function. In this case, the authors prefer the trainrp function with a large number of epochs yet small error values because the important aspect of forecasting is the level of accuracy produced. It is in accordance with the statement in the study [75] that the number of training times, known as "epoch" in deep learning, had no effect on the performance of the trained forecast model and it exhibited a truly random behavior. In general, the results of data training and testing showed that the MAPE values of temperature and humidity data were still classified as indicating highly accurate forecasting, while wind speed and sunshine data were classified as indicating good forecasting.

In addition, the BP-RVM algorithm provided good results when training and testing temperature, wind speed and humidity data since these three data include stable and static data, while rainfall and sunshine data are two interrelated data and include non-static data. Therefore, the MSE and MAPE values were relatively large. This shows that it is important to take into account data stability when forecasting. This result is supported by Hardt et al. [76] when testing neural network algorithms on larger data. They found that static types of data provided relatively small error values compared to data with a highly fluctuating trend.

4.3 Trends of hydro-climatology data

The results of data training and testing in Table 1 and Table 2 led the authors to use the BP-RVM algorithm with the RBF-trainrp function combination for future data prediction. Data prediction was carried out to determine the climate change that occurred at Kediri Station area in West Lombok, Indonesia based on the Oldeman classification. The prediction output consisted of 36 data, so the authors calculated every three data into one month data. During the calculation process, the authors summed the rainfall data and calculated the average of tempetature, humidity, wind speed, and sunshine duration data. The results of data prediction can be seen in Table 3.

Based on Table 3, it was predicted that the maximum rainfall value would occur in December with 467.60 mm and the minimum value would occur in September with 22.63 mm. The classification results showed that there would be 5 wet months, 3 humid months, and 4 dry months. Referring to the Oldeman classification and considering the data pattern from the previous year to December 2022, this region falls into classification D that has 4 consecutive wet months. Second, the prediction results of temperature data showed that 9 months are categorized as "hot" and 3 months are categorized as “tropical”, with an average temperature of 26.55℃ per month. Third, the prediction results of humidity data showed that the entire year is included in the "humid" category with an average of 84.20%. Fourth, the prediction results of wind speed data obtained an average of 3.02 m/s, categorizing the wind in the region into the "light breeze" category with 8 months of "light breeze" and 4 months of "gentle breeze". Finally, the prediction results of sunshine duration data showed that there would be a significant increase from the MAM period to the JJA period and a decrease in the SON period and the DJF period.

Table 3. Prediction results of hydro-climatological data from Kediri Station in West Lombok, Indonesia

Month	Rainfall (mm)		Temperature (℃)		Air Humidity (%)		Wind Speed (m/s)		Sunshine (%)	
	Data	Category	Data	Category	Data	Category	Data	Category	Data	Category
1	344.72	Wet	26.70	Hot	85.44	Humid	1.58	Light	46.49	DJF
2	294.52	Wet	26.69	Hot	86.18	Humid	2.12	Light	67.41	
3	132.86	Humid	27.46	Hot	82.09	Humid	2.41	Light	59.53	
4	239.01	Wet	27.18	Hot	80.29	Humid	2.18	Light	84.09	MAM
5	175.88	Humid	26.43	Hot	84.64	Humid	2.75	Light	88.25	
6	176.61	Humid	25.34	Tropical	86.20	Humid	2.75	Light	76.60	
7	82.57	Dry	24.93	Tropical	84.29	Humid	4.16	Gentle	82.69	JJA
8	52.50	Dry	25.53	Tropical	83.06	Humid	4.56	Gentle	82.86	
9	22.63	Dry	26.61	Hot	82.40	Humid	4.95	Gentle	78.05	
10	92.16	Dry	27.54	Hot	82.72	Humid	3.67	Gentle	67.37	SON
11	225.38	Wet	27.16	Hot	87.00	Humid	2.37	Light	47.04	
12	467.60	Wet	27.07	Hot	86.09	Humid	2.70	Light	49.38	DJF

In theory, the elements of climate or weather influence each other, such as rainfall, temperature, humidity, and sunshine duration [77, 78]. In Table 3, an increase in rainfall is characterized by a relatively short sunshine duration. The relatively short sunshine duration will impact the temperature in the region. Meanwhile, temperature will affect humidity [79]. These weather or climate changes are used as an important basis in agriculture, especially in planning cropping patterns.

5. CONCLUSIONS

The hybrid backpropagation-relevance vector machine (BP-RVM) with a Radial Basis Function (RBF) kernel function demonstrated superior performance compared to other algorithms, as evidenced by its relatively small Mean Squared Error (MSE) and Mean Absolute Percentage Error (MAPE) values, which categorize it as a highly accurate forecast model.

In our experiment, the combination of the RBF-trainrp kernel function nearly doubled the speed of the training-testing process compared to the logsig-trainrp function. While the RBF-trainlm kernel function combination enhanced the speed of the training-testing process sixfold, we do not recommend its use due to the resultant increase in the MSE and MAPE values for each prediction result.

These outcomes suggest that substituting input data into the RBF function following the BP-RVM algorithm leads to more accurate performance than the BP and BP-RBF algorithms. Additionally, implementing the RBF function as the activation function in the first hidden layer expedited the data centering process. Hence, we recommend the BP-RVM-RBF algorithm architecture for forecasting various types of hydroclimatological data, such as determining the effective rainfall volume, evapotranspiration, and crop water requirements, which are crucial for designing future cropping patterns.

However, we observed inconsistencies in the number of neurons in each layer when the RBF function was applied to each hidden layer during the experiment. This finding warrants further investigation in future research.

REFERENCES

[1] Wang, H., Liu, L., Qian, Z., Wei, H., Dong, S. (2014). Empirical mode decomposition-autoregressive integrated moving average: Hybrid short-term traffic speed prediction model. Transportation Research Record, 2460(1): 66-76. https://doi.org/10.3141/2460-08

[2] Xue, B., Zhang, M., Browne, W.N., Yao, X. (2016). A survey on evolutionary computation approaches to feature selection. IEEE Transactions on Evolutionary Computation, 20(4): 606-626. https://doi.org/10.1109/TEVC.2015.2504420

[3] Thakur, B., Kalra, A., Ahmad, S., Lamb, K.W., Lakshmi, V. (2020). Bringing statistical learning machines together for hydro-climatological predictions - Case study for Sacramento San joaquin River Basin, California. Journal of Hydrology: Regional Studies, 27: 100651. https://doi.org/10.1016/j.ejrh.2019.100651

[4] Abdi, M.J., Raffar, N., Zulkafli, Z., Nurulhuda, K., Rehan, B.M., Muharam, F.M., Khosim, N.A., Tangang, F. (2022). Index-based insurance and hydroclimatic risk management in agriculture: A systematic review of index selection and yield-index modelling methods. International Journal of Disaster Risk Reduction, 67: 102653. https://doi.org/10.1016/j.ijdrr.2021.102653

[5] Walthall, C., Anderson, C., Takle, E., Baumgard, L., Wright-Morton, L. (2013). Climate change and agriculture in the United States: Effects and adaptation. USDA Technical Bulletin 1935, February, i – 186.

[6] Rakhecha, P.R., Singh, V.P. (2009). Applied hydrometeorology. In Applied Hydrometeorology. https://doi.org/10.1007/978-1-4020-9844-4

[7] Doraiswamy, P.C., Pasteris, P.A., Jones, K.C., Motha, R.P., Nejedlik, P. (2000). Techniques for methods of collection, database management and distribution of agrometeorological data. Agricultural and Forest Meteorology, 103(1-2): 83-97. https://doi.org/10.1016/S0168-1923(00)00120-9

[8] Syaharuddin, Pramita, D., Nusantara, T., Subanji, Negara, H.R.P. (2020). Analysis of accuracy parameters of ANN backpropagation algorithm through training and testing of hydro-climatology data based on GUI MATLAB. IOP Conference Series: Earth and Environmental Science, 413(1): 012008. https://doi.org/10.1088/1755-1315/413/1/012008

[9] Traore, S., Wang, Y.M., Kerh, T. (2010). Artificial neural network for modeling reference evapotranspiration complex process in Sudano-Sahelian zone. Agricultural Water Management, 97(5): 707-714. https://doi.org/10.1016/j.agwat.2010.01.002

[10] Mislan, Haviluddin, Hardwinarto, S., Sumaryono, Aipassa, M. (2015). Rainfall monthly prediction based on artificial neural network: A case study in Tenggarong

Station, East Kalimantan - Indonesia. Procedia Computer Science, 59: 142-151. https://doi.org/10.1016/j.procs.2015.07.528
[11] Ramseyer, C.A., Miller, P.W., Mote, T.L. (2019). Future precipitation variability during the early rainfall season in the El Yunque National Forest. Science of the Total Environment, 661: 326-336. https://doi.org/10.1016/j.scitotenv.2019.01.167
[12] Kashid, S.S., Maity, R. (2012). Prediction of monthly rainfall on homogeneous monsoon regions of India based on large scale circulation patterns using Genetic Programming. Journal of Hydrology, 454-455: 26-41. https://doi.org/10.1016/j.jhydrol.2012.05.033
[13] Irawan, M.I., Syaharuddin, Utomo, D.B., Rukmi, A.M. (2013). Intelligent irrigation water requirement system based on artificial neural networks and profit optimization for planting time decision making of crops in Lombok Island. Journal of Theoretical and Applied Information Technology, 58(3): 657-671.
[14] Sachindra, D.A., Ahmed, K., Rashid, M.M., Shahid, S., Perera, B.J.C. (2018). Statistical downscaling of precipitation using machine learning techniques. Atmospheric Research, 212: 240-258. https://doi.org/10.1016/j.atmosres.2018.05.022
[15] Foody, G.M. (2008). RVM-based multi-class classification of remotely sensed data. International Journal of Remote Sensing, 29(6): 1817-1823. https://doi.org/10.1080/01431160701822115
[16] Caesarendra, W., Widodo, A., Yang, B.S. (2010). Application of relevance vector machine and logistic regression for machine degradation assessment. Mechanical Systems and Signal Processing, 24(4): 1161-1171. https://doi.org/10.1016/j.ymssp.2009.10.011
[17] Quiñonero-Candela, J., Hansen, L.K. (2002). Time series prediction based on the relevance vector machine with adaptive kernels. In ICASSP, IEEE International Conference on Acoustics, Speech and Signal Processing - Proceedings, Orlando, FL, USA, pp. I-985-I-988. https://doi.org/10.1109/icassp.2002.5743959
[18] Bonanno, F., Capizzi, G., Graditi, G., Napoli, C., Tina, G.M. (2012). A radial basis function neural network based approach for the electrical characteristics estimation of a photovoltaic module. Applied Energy, 97: 956-961. https://doi.org/10.1016/j.apenergy.2011.12.085
[19] Song, X., Duan, Z., Jiang, X. (2012). Comparison of artificial neural networks and support vector machine classifiers for land cover classification in Northern China using a SPOT-5 HRG image. International Journal of Remote Sensing, 33(10): 3301-3320. https://doi.org/10.1080/01431161.2011.568531
[20] Nitze, I., Schulthess, U., Asche, H. (2012). Comparison of machine learning algorithms random forest, artificial neuronal network and support vector machine to maximum likelihood for supervised crop type classification. In Proceedings of the 4th Conference on GEographic Object-Based Image Analysis – GEOBIA 2012, pp. 35-40.
[21] Ghorbani, M.A., Zadeh, H.A., Isazadeh, M., Terzi, O. (2016). A comparative study of artificial neural network (MLP, RBF) and support vector machine models for river flow prediction. Environmental Earth Sciences, 75(6): 476. https://doi.org/10.1007/s12665-015-5096-x
[22] Du, K.L., Swamy, M.N.S., Du, K.L., Swamy, M.N.S. (2014). Fundamentals of machine learning. In Neural Networks and Statistical Learning, pp. 15-65. https://doi.org/10.1007/978-1-4471-5571-3_2
[23] Russell, S., Norvig, P. (2010). Artificial Intelligence A Modern Approach Third Edition. In Pearson. https://doi.org/10.1017/S0269888900007724
[24] Syaharuddin, Fatmawati, Suprajitno, H. (2022b). Experimental analysis of training parameters combination of ANN backpropagation for climate classification. Mathematical Modelling of Engineering Problems, 9(4): 994-1004. https://doi.org/https://doi.org/10.18280/mmep.090417
[25] Mondal, B., Meetei, M.S., Das, J., Roy Chaudhuri, C., Saha, H. (2015). Quantitative recognition of flammable and toxic gases with artificial neural network using metal oxide gas sensors in embedded platform. Engineering Science and Technology, an International Journal, 18(2): 229-234. https://doi.org/10.1016/j.jestch.2014.12.010
[26] Ellah, A.R.A., Essai, M.H., Yahya, A. (2016). Comparison of different backpropagation training algorithms using robust M-estimators performance functions. In Proceedings - 2015 10th International Conference on Computer Engineering and Systems, ICCES 2015, pp. 384–388. https://doi.org/10.1109/ICCES.2015.7393080
[27] Almawla, A.S., Lateef, A.M., Kamel, A.H. (2022). Modelling the effects of hydraulic force on strain in hydraulic structures using ANN (Haditha Dam in Iraq as a case study). Mathematical Modelling of Engineering Problems, 9(1): 150-158. https://doi.org/10.18280/mmep.090119
[28] Makwana, M.A., Patolia, H.P. (2021). Forward kinematics of delta manipulator by novel hybrid neural network. international journal of mathematical, engineering and Management Sciences, 6(6): 1694-1708. https://doi.org/10.33889/IJMEMS.2021.6.6.100
[29] Kannaiyan, M., Karthikeyan, G., Thankachi Raghuvaran, J.G. (2020). Prediction of specific wear rate for LM25/ZrO_2 composites using Levenberg-Marquardt backpropagation algorithm. Journal of Materials Research and Technology, 9(1): 530-538. https://doi.org/10.1016/j.jmrt.2019.10.082
[30] Ahmad, F., Yahya, S.Z., Saad, Z., Ahmad, A.R. (2018). Tajweed classification using artificial neural network. In 2018 International Conference on Smart Applications, Communications and Networking, SmartNets 2018. https://doi.org/10.1109/SMARTNETS.2018.8707394
[31] Rezaei, J., Shahbakhti, M., Bahri, B., Aziz, A.A. (2015). Performance prediction of HCCI engines with oxygenated fuels using artificial neural networks. Applied Energy, 138: 460-473. https://doi.org/10.1016/j.apenergy.2014.10.088
[32] Lahmiri, S. (2011). A comparative study of backpropagation algorithms in financial prediction. International Journal of Computer Science, Engineering and Applications (IJCSEA), 1(4): 15-21. https://airccse.org/journal/ijcsea/current.html
[33] Tipping, M. E. (2001). Sparse Bayesian learning and the relevance vector machine. Journal of Machine Learning Research, 1(3): 211-244. https://doi.org/https://doi.org/10.1162/15324430152748236
[34] Jing, B., Qian, Z., Wang, A., Chen, T., Zhang, F. (2020). Wind turbine power curve modelling based on hybrid

relevance vector machine. Journal of Physics: Conference Series, 1659(1): 012034. https://doi.org/10.1088/1742-6596/1659/1/012034
[35] Chen, S., Gu, C., Lin, C., Zhang, K., Zhu, Y. (2021). Multi-kernel optimized relevance vector machine for probabilistic prediction of concrete dam displacement. Engineering with Computers, 37(3): 1943-1959. https://doi.org/10.1007/s00366-019-00924-9
[36] Tao, H., Al-Bedyry, N.K., Khedher, K.M., Shahid, S., Yaseen, Z.M. (2021). River water level prediction in coastal catchment using hybridized relevance vector machine model with improved grasshopper optimization. Journal of Hydrology, 598: 126477. https://doi.org/10.1016/j.jhydrol.2021.126477
[37] Chen, L., Zhao, J., Wang, W., Xu, Q. (2021). A Gaussian approximation of marginal likelihood in relevance vector machine for industrial data with input noise. IEEE Transactions on Instrumentation and Measurement, 70: 2501212. https://doi.org/10.1109/TIM.2020.3017955
[38] Liu, Y., Ye, Y., Wang, Q., Liu, X., Wang, W. (2019). Predicting the loose zone of roadway surrounding rock usingwavelet relevance vector machine. Applied Sciences (Switzerland), 9(10): 2064. https://doi.org/10.3390/app9102064
[39] Shobitha, S., Amita, P.M., Krupa, B.N., Beng, G.K. (2018). Cuffless blood pressure prediction from PPG using relevance vector machine. In International Conference on Electrical, Electronics, Communication Computer Technologies and Optimization Techniques, ICEECCOT 2017, pp. 75-78. https://doi.org/10.1109/ICEECCOT.2017.8284610
[40] Gayathri, B.M., Sumathi, C.P. (2017). Comparative study of relevance vector machine with various machine learning techniques used for detecting breast cancer. 2016 IEEE International Conference on Computational Intelligence and Computing Research, Chennai, India, 2016, pp. 1-5. https://doi.org/10.1109/ICCIC.2016.7919576
[41] Yuvaraj, P., Murthy, A.R., Iyer, N.R., Samui, P., Sekar, S.K. (2014). Prediction of fracture characteristics of high strength and ultra high strength concrete beams based on relevance vector machine. International Journal of Damage Mechanics, 23(7): 979-1004. https://doi.org/10.1177/1056789514520796
[42] Bowd, C., Lee, I., Goldbaum, M.H., Balasubramanian, M., Medeiros, F.A., Zangwill, L.M., Girkin, C.A., Liebmann, J.M., Weinreb, R.N. (2012). Predicting glaucomatous progression in glaucoma suspect eyes using relevance vector machine classifiers for combined structural and functional measurements. Investigative Ophthalmology and Visual Science, 53(4): 2382-2389. https://doi.org/10.1167/iovs.11-7951
[43] Ge, Z., Song, Z. (2010). Nonlinear soft sensor development based on relevance vector machine. Industrial and Engineering Chemistry Research, 49(18): 8685-8693. https://doi.org/10.1021/ie101146d
[44] Guo, S., Zhao, H., Zhao, H. (2017). A new hybridwind power forecaster using the beveridge-nelson decomposition method and a relevance vector machine optimized by the ant lion optimizer. Energies, 10(7): 922. https://doi.org/10.3390/en10070922
[45] Agrawal, R.K., Muchahary, F., Tripathi, M.M. (2019). Ensemble of relevance vector machines and boosted trees for electricity price forecasting. Applied Energy, 250: 540-548. https://doi.org/10.1016/j.apenergy.2019.05.062
[46] Bing, Q., Gong, B., Yang, Z., Shang, Q., Zhou, X. (2015). Short-term traffic flow local prediction based on combined kernel function relevance vector machine model. Mathematical Problems in Engineering, 2015: 154703. https://doi.org/10.1155/2015/154703
[47] Swati, S., Kumar, M., Mishra, R.K. (2019). Classification of microarray data using kernel based classifiers. Revue d'Intelligence Artificielle, 33(3): 235-247. https://doi.org/10.18280/ria.330310
[48] Yu, Z., Shi, X., Zhou, J., Gou, Y., Huo, X., Zhang, J., Armaghani, D.J. (2020). A new multikernel relevance vector machine based on the HPSOGWO algorithm for predicting and controlling blast-induced ground vibration. Engineering with Computers, 38: 1905-1920. https://doi.org/10.1007/s00366-020-01136-2
[49] Kara, Y., Acar Boyacioglu, M., Baykan, Ö.K. (2011). Predicting direction of stock price index movement using artificial neural networks and support vector machines: The sample of the Istanbul Stock Exchange. Expert Systems with Applications, 38(5): 5311-5319. https://doi.org/10.1016/j.eswa.2010.10.027
[50] Wei, P., Li, Z., Li, X., Wang, M.Y. (2018). An 88-line MATLAB code for the parameterized level set method based topology optimization using radial basis functions. Structural and Multidisciplinary Optimization, 58(2): 831-849. https://doi.org/10.1007/s00158-018-1904-8
[51] González-Camacho, J.M., de los Campos, G., Pérez, P., Gianola, D., Cairns, J.E., Mahuku, G., Babu, R., Crossa, J. (2012). Genome-enabled prediction of genetic values using radial basis function neural networks. Theoretical and Applied Genetics, 125(4): 759-771. https://doi.org/10.1007/s00122-012-1868-9
[52] Razaque, A., Ben Haj Frej, M., Almi'ani, M., Alotaibi, M., Alotaibi, B. (2021). Improved support vector machine enabled radial basis function and linear variants for remote sensing image classification. Sensors, 21(13): 4431. https://doi.org/10.3390/s21134431
[53] Syaharuddin, Fatmawati, Suprajitno, H. (2022). The formula study in determining the best number of neurons in neural network backpropagation architecture with three hidden layers. Jurnal RESTI (Rekayasa Sistem Dan Teknologi Informasi), 6(3): 397-402. https://doi.org/https://doi.org/10.29207/resti.v6i3.4049
[54] Syaharuddin, Fatmawati, Suprajitno, H. (2022). Best architecture recommendations of ANN backpropagation based on combination of learning rate, momentum, and number of hidden layers. JTAM (Jurnal Teori Dan Aplikasi Matematika), 6(3): 629-637. https://doi.org/10.31764/jtam.v6i3.8524
[55] Abhishek, K., Kumar, A., Ranjan, R., Kumar, S. (2012). A rainfall prediction model using artificial neural network. In Proceedings - 2012 IEEE Control and System Graduate Research Colloquium, Shah Alam, Malaysia, pp. 82-87. https://doi.org/10.1109/ICSGRC.2012.6287140
[56] Ogasawara, E., Martinez, L.C., De Oliveira, D., Zimbrão, G., Pappa, G.L., Mattoso, M. (2010). Adaptive Normalization: A novel data normalization approach for non-stationary time series. In Proceedings of the International Joint Conference on Neural Networks, Barcelona, Spain, pp. 1-8. https://doi.org/10.1109/IJCNN.2010.5596746

[57] Khond, S.V. (2020). Effect of data normalization on accuracy and error of fault classification for an electrical distribution system. Smart Science, 8(3): 117-124. https://doi.org/10.1080/23080477.2020.1799135
[58] Nayak, S.C., Misra, B.B., Behera, H.S. (2014). Impact of data normalization on stock index forecasting. International Journal of Computer Information Systems and Industrial Management Applications, 6(2014): 257-269. www.mirlabs.net/ijcisim/index.html
[59] Wijaya, A., Surahman, M., Susantidiana, S., Lakitan, B. (2014). Genetic relationships among indonesian *jatropha curcas* L. Accessions, selected crossings, and seed oil yield of their progenies. Chiang Mai Journal of Science, 41(5-1): 1109-1120.
[60] Oldeman, L., Suardi, D. (1977). Climatic Determinants in Relation to Cropping Patterns. The International Rice Research Institute.
[61] Ahmada, B., Rahmah, C.N., Larasati, L.A., Muchlis, L., Qonita, M., Khoiruluswati, N.M., Rohmah, S., Karunia Rahayu, T.D., Nurjani, E. (2020). Climate-based crop pattern determination using Standard Precipitation Index (SPI) and the Oldeman classification in Sangiran Site. IOP Conference Series: Earth and Environmental Science, 451(1): 012019. https://doi.org/10.1088/1755-1315/451/1/012019
[62] Junghuhn, F.W. (1845). Die Topographischen und Naturwissenschaftlichen Reisen Durch Java. Engelmann.
[63] Sari, D.P., Simanungkalit, N.M., Novira, N. (2021). Landslide susceptibility mapping in berastagi district karo regency based on geographic information systems. Tunas Geografi, 10(1): 9. https://doi.org/10.24114/tgeo.v10i1.27902
[64] Santosa, E., Susila, A.D., Widodo, W.D., Nasrullah, N., Ruwaida, I.P., Sari, R. (2021). Exploring fruit tree species as multifunctional greenery: A case of its distribution in indonesian cities. Sustainability (Switzerland), 13(14): 7835. https://doi.org/10.3390/su13147835
[65] Radinović, D., Ćurić, M. (2014). Measuring scales for daily temperature extremes, precipitation and wind velocity. Meteorological Applications, 21(3): 461-465. https://doi.org/10.1002/met.1356
[66] Tahbaz, M. (2009). Estimation of the wind speed in urban areas - Height less than 10 metres. International Journal of Ventilation, 8(1): 75-84. https://doi.org/10.1080/14733315.2006.11683833
[67] Penwarden, A., Wise, A. (1975). Wind Environment Around Buildings. Building Research Establishment Report.
[68] McMurry, P.H., Stolzenburg, M.R. (1989). On the sensitivity of particle size to relative humidity for Los Angeles aerosols. Atmospheric Environment (1967), 23(2): 497-507. https://doi.org/10.1016/0004-6981(89)90593-3
[69] Arundel, A.V., Sterling, E.M., Biggin, J.H., Sterling, T.D. (1986). Indirect Health Effects of Relative Humidity in Indoor Environments. Environmental Health Perspectives, 65: 351. https://doi.org/10.2307/3430203
[70] Zahradníček, P., Brázdil, R., Štěpánek, P., Trnka, M. (2021). Reflections of global warming in trends of temperature characteristics in the Czech Republic, 1961–2019. International Journal of Climatology, 41(2): 1211-1229. https://doi.org/10.1002/joc.6791
[71] Brázdil, R., Zahradníček, P., Dobrovolný, P., Štěpánek, P., Trnka, M. (2021). Observed changes in precipitation during recent warming: The Czech Republic, 1961–2019. International Journal of Climatology, 41(7): 3881-3902. https://doi.org/10.1002/joc.7048
[72] Lewis, C.D. (1982). Industrial and business forecasting methods. Butterworths, London. https://doi.org/10.1002/for.3980020210
[73] Yadav, V., Nath, S. (2017). Forecasting of PM Models and Exponential Smoothing Technique. Asian Journal of Water, Environment and Pollution, 14(4): 109-113. https://doi.org/10.3233/AJW-170041
[74] Montaño Moreno, J.J., Palmer Pol, A., Sesé Abad, A., Cajal Blasco, B. (2013). Using the R-MAPE index as a resistant measure of forecast accuracy. Psicothema, 25(4): 500-506. https://doi.org/10.7334/psicothema2013.23
[75] Siami-Namini, S., Tavakoli, N., Siami Namin, A. (2019). A comparison of ARIMA and LSTM in forecasting time series. In Proceedings - 17th IEEE International Conference on Machine Learning and Applications, ICMLA 2018, pp. 1394-1401. https://doi.org/10.1109/ICMLA.2018.00227
[76] Hardt, M., Recht, B., Singer, Y. (2016). Train faster, generalize better: Stability of stochastic gradient descent. In the 33rd International Conference on Machine Learning, ICML 2016, pp. 1868-1877.
[77] Ngondjeb, Y.D. (2013). Agriculture and climate change in cameroon: An assessment of impacts and adaptation options. African Journal of Science, Technology, Innovation and Development, 5(1): 85-94. https://doi.org/10.1080/20421338.2013.782151
[78] Lambi, C., Forbang, T. (2009). The economic impact of climate change on agriculture in Cameroon. IOP Conference Series: Earth and Environmental Science, 6(9): 092017. https://doi.org/10.1088/1755-1307/6/9/092017
[79] Berndt, C., Haberlandt, U. (2018). Spatial interpolation of climate variables in Northern Germany—Influence of temporal resolution and network density. Journal of Hydrology: Regional Studies, 15: 184-202. https://doi.org/10.1016/j.ejrh.2018.02.002